

Development of anisotropy in ultra-high molecular weight polyethylene

P. Gao, M. R. Mackley* and T. M. Nicholson

Department of Chemical Engineering, University of Cambridge, Pembroke Street, Cambridge CB2 3RA, UK

(Received 1 February 1989; revised 26 April 1989; accepted 5 June 1989)

We report experimental measurements on the drawing behaviour of a pre-swollen drawn sample of ultra-high molecular weight polyethylene (UHMWPE). X-ray information is expressed in terms of an orientation function $P_2(\theta)$, and the increase in both P_2 and the tensile modulus are determined as a function of draw ratio. Scanning electron microscopy is used to follow the structural changes in the material. The experimental results are compared with a numerical simulation of the deformation and from these we suggest that early stages of deformation involve crystal orientation followed by subsequent chain extension at higher draw ratios.

(Keywords: swelling; ultrahigh molecular weight polyethylene; X-ray analysis high modulus; mechanical properties; aggregate model)

INTRODUCTION

Within the last ten years a number of related processing routes have been discovered for manufacturing high strength and stiffness polyethylene structures using ultra-high molecular weight polyethylene (UHMWPE) precursor material. Zwiijnenburg and Pennings¹ developed a surface growth process where the fibres were crystallized and drawn directly from a polyethylene solution. Smith and Lemstra² pioneered the gel spinning technology where a 'low entanglement' gel fibre is spun and then crystallized; the solvent is removed and anisotropy generated in the fibre by means of hot drawing. Other process routes have been reported which include variants of gel spinning^{3,4}, ram extrusion of 'low entanglement' UHMWPE⁵⁻⁷, drawing of reactor UHMWPE material^{8,9}, die free spinning¹⁰ and the swell drawing of UHMWPE¹¹. The swell draw process involves starting with an isotropic solid piece of material. The polymer is then swollen using an appropriate solvent, temperature and time such that high swelling ratios are achieved without the material losing its mechanical integrity. In the swollen state it is assumed that the level of entanglement within the material is reduced. The low entanglement concentration is further assumed to be trapped within the material when the swollen material is quenched and crystallization occurs. After solvent removal, anisotropy is developed by hot drawing the material. It has been found that the pre-swelling of the polymer greatly enhances the material's ability to be drawn above its natural draw ratio¹¹ and correspondingly the tensile properties are also enhanced⁷.

The primary purpose of this paper is to describe experimental observations we have made on a swell drawn UHMWPE sample and discuss these results in terms of the possible deformation mechanisms occurring within the material at different stages in the drawing process. A number of authors have attempted to describe the deformation behaviour of polymers^{12,13} and recently Termonia and Smith¹⁴ have developed a numerical simulation of drawing behaviour which covers drawing

both for normally 'entangled' and 'low entanglement' materials.

EXPERIMENTAL

Swelling, quenching, crystallization and solvent removal

The polymer used in this study was UHMWPE HG415 manufactured by Hoechst. Tapes of 0.5 mm thickness were used and they were supplied by Performance Plastic Ltd (Bacup, UK) from slabs that had been prepared by ram extrusion. Specimens were annealed for 25 min at 150°C and oven cooled to relieve any residual thermal and mechanical history. Swelling was done by immersing preweighed specimens in a solvent bath of decalin which was maintained at the appropriate temperature by a silicon oil bath. After chosen times, specimens were removed from the bath and weighed with a microbalance which was connected to a chart recorder. The weight was measured as a function of time and the total swollen weight obtained by extrapolating the curve to zero time (solvent loss between immersion and weighing was < 1%). *Figure 1* shows the observed weight uptake for decalin solvent as a function of time; the experiments were conducted at 125°C. The experimental data is plotted in terms of W_s/W_p as a function of time, where W_s is the solvent weight within the polymer at time t and W_p the initial weight of the polymer sample. The plot shows an essentially linear weight uptake as a function of time and the ability to achieve high solvent loadings is apparent.

Quenching of the swollen samples was achieved by removing the sample from the bath and cooling in the ambient conditions. We estimate that the material would have cooled from the bath temperature of 125°C to an appropriate crystallization temperature of say 80°C within 5 s. The crystallized gel samples were left to dry at ambient conditions for ≈ 12 h, and then they were transferred to a JJ environmental cabinet and held at 80°C for ≈ 20 min to enhance solvent evaporation. The nearly dried gel films were finally immersed in an excess of acetone and subsequently air dried to remove residual

* To whom correspondence should be addressed

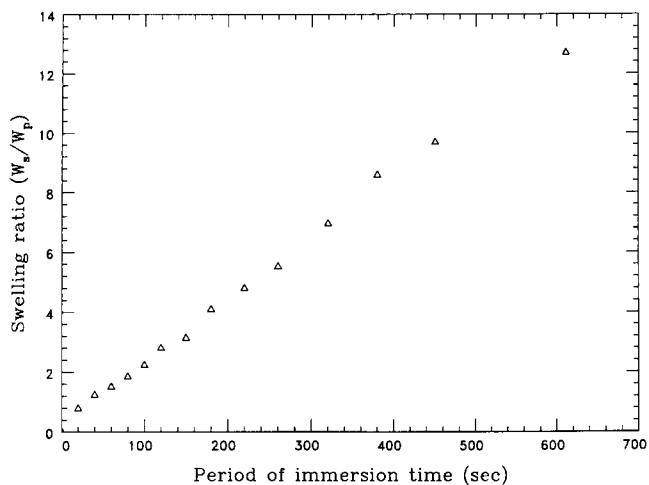


Figure 1 Solvent weight uptake versus immersion time for 0.5 mm thick HG415 tapes in decalin; swelling temperature 125°C

traces of decalin-acetone mixture. We estimate that before drawing the residual solvent content was <2%. The dried gel films were cut into dumb-bell shaped specimens with a gauge length of 25 mm and a width of 4 mm for the drawing experiment.

Drawing

The hot drawing behaviour of the samples was studied using a JJ tensile drawing testing machine equipped with an environmental cabinet. Drawing was performed under isothermal conditions at a constant crosshead speed of 100 mm min⁻¹. Draw ratios λ were determined in the usual way by measuring the displacement of ink marks placed 20 mm apart on the specimen before drawing. Elongation of $\lambda > 10$ was carried out as a multi-stage process, because of a length constraint of the environmental cabinet. The specimen was drawn to $\lambda = 10$ in the first stage and the drawn film was then cut into strips of length of 80–90 mm. These specimens were subsequently clamped over a length of 50 mm and further drawn to about 200 mm in a second stage. In this way draw ratios between $\lambda = 10$ and $\lambda = 40$ could be explored. Results reported in this paper relate to a single initial swelling condition of decaline immersion for 440 s at 125°C. These samples were then drawn to different draw ratio at 120°C. Under these conditions it was found that the maximum draw ratio that could be achieved was 40.

Scanning electron microscopy (SEM) observation

SEM photographs of the free surface of the swell drawn material are shown in Figure 2. Figure 2a shows the undrawn pre-swollen starting material. The material shows evidence of porosity and unoriented lamellar crystals appear to be present. We saw no direct evidence to suggest that spherulitic crystallization had occurred. At a modest draw ratio of 5, as shown in Figure 2b, a transition between a lamellar and a fibrillar texture appeared to be occurring. At high draw ratios, as shown in Figures 2c and d, the fibrillar texture dominated, with the orientation and clarity of the fibrous entities increasing with increasing draw ratio.

X-ray measurements

Wide angle X-ray diffraction (WAXD) patterns were obtained using a flat film camera and CuK_α radiation

at 30 mA and 40 kV. The X-ray beam was made monochromatic by using a nickel filter to give a wavelength of 0.15417 nm. The exposure time for all the specimens was 25 min, and the working distance between sample and film was 30 mm. Figure 3 shows the evolution of the X-ray diffraction pattern as a function of draw ratio. Figure 3a shows the typical polyethylene diffraction rings for unoriented material. Drawing induces molecular orientation, which leads to the equatorial concentration of scattering intensity for the 200, 020 and 110 diffraction peaks, as shown in Figure 3c and d.

The variation of intensity around the appropriate arc of the diffraction pattern was determined by using an image analyser. The relative intensity around arcs (200) and (020) (i.e. $I(\phi)_{200}$ and $I(\phi)_{020}$) was obtained by a scan determining the scattering intensity $I(\phi)$ at a position (x, y) on the photograph negative, where $x^2 + y^2 = R^2$ and R is the radius of the diffraction arc. The intensity was measured at 1° increments around the arcs and the value of the orientation function $P_2(\theta)$ was computed from the intensity measurements using the method described by Stein¹⁵, which is summarized in the Appendix to this paper.

Mechanical properties measurements

The Young's modulus and strength of the drawn tapes were measured at room temperature ($\approx 20^\circ\text{C}$). Samples of initial length 150–170 mm and a crosshead speed of 100 mm min⁻¹ were used, and measurements were taken at the point of the maximum slope on the load-deflection graph. Errors in each measurement are estimated to be of the order of $\pm 10\%$.

MODELLING DRAW BEHAVIOUR

We have chosen to simulate the drawing behaviour of the pre-swollen polymer by using the aggregate model and pseudo-affine deformation, which has been successfully used by other workers to describe the deformation of melt crystallized semicrystalline polymers^{12,16,17}. In the aggregate model the material is assumed to be composed of an aggregate of elastically anisotropic units. Each of these units is assigned elastic properties which are assumed to be independent of deformation. For any given distribution of orientations of these units the orientation function and the tensile modulus may be calculated.

Initially a random distribution of orientations is generated, corresponding to the undrawn polymer. The draw process is then modelled by applying a pseudo-affine deformation, the orientation in each unit being altered as if the vectors describing these orientations were embedded in a substrate that is uniformly drawn without change of volume (Figure 4). Changes in the length of the vectors are ignored; only the resulting directions are considered. At each draw ratio, the orientation function and tensile modulus were then calculated from the distribution of unit orientations. The same results were obtained regardless of whether the orientation distribution was generated by applying a single step deformation, or as the product of several smaller draw deformations. An array of 2000 units was used in the simulations described here.

The orientation function corresponding to a given distribution can be calculated simply by computing the

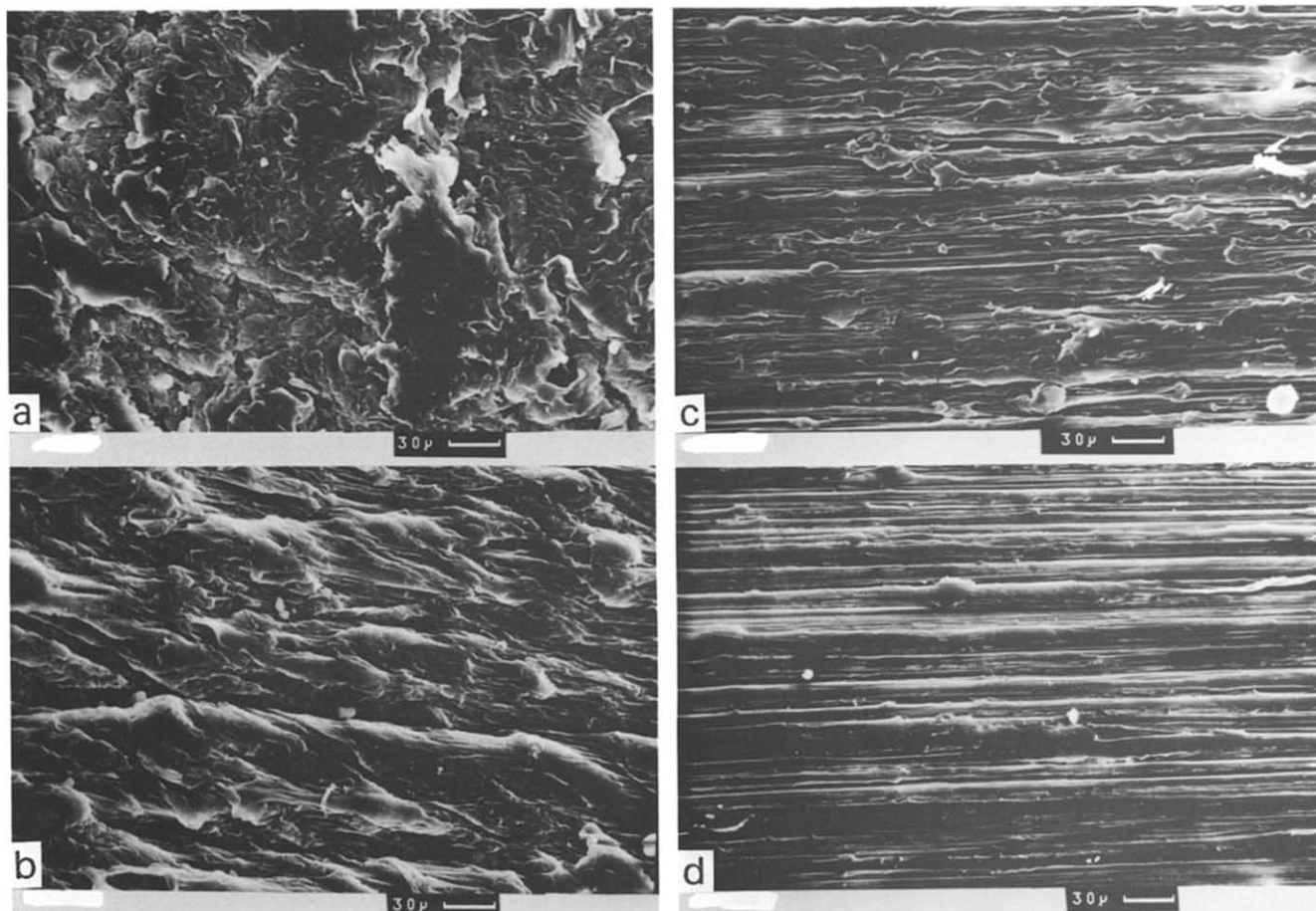


Figure 2 Scanning electron micrographs of drawn UHMWPE films with draw ratios λ of (a) 1.0, (b) 5.0, (c) 15.0 and (d) 40.0. The stretching direction is horizontal

average

$$P_2 = \frac{1}{2} \langle 3 \cos^2 \alpha - 1 \rangle \quad (1)$$

where α is the angle between the orientation of a particular cell and the draw direction and the angle brackets indicate averaged quantities. Results from such calculations are shown in *Figure 5*, superimposed on the experimental data obtained by analysis of the X-ray results. A striking agreement is obtained between the experimental data and the numerical prediction.

The tensile modulus is calculated by averaging elastic constants throughout the aggregate. This may be done in two limiting ways¹⁶, either by assuming a uniform stress throughout the material (effectively placing the units in series) or by assuming a uniform strain (corresponding to a parallel coupling of the units).

The first method involves an averaging of compliance coefficients. Using tensor transformations, the extensional compliance along the draw direction in each unit, s'_{33} , may be calculated in terms of the compliance coefficients along the major axes of a unit cell, which in turn are related to physical properties of the highly oriented polymer (*Table 1*). The extensional strain in this unit e is related to the stress σ by the expression $e = s'_{33}\sigma$. Averaging over all the units gives $\langle e \rangle = \langle s'_{33} \rangle \sigma$ and hence the tensile modulus E is given by

$$E = \frac{\sigma}{\langle e \rangle} = \frac{1}{\langle s'_{33} \rangle} \quad (2)$$

The alternative method of calculating the tensile modulus for a given distribution of unit orientations involves an averaging of stiffness coefficients and leads to a second expression for the tensile modulus:

$$E = \langle c'_{33} \rangle \quad (3)$$

where c'_{33} is the extensional stiffness along the draw direction of a particular unit. This can be calculated again by tensor methods from the principle stiffness coefficients for a unit cell. These stiffness coefficients are related numerically to the compliance coefficients.

These two methods yield an upper and lower bound¹⁸ for the mechanical response. The behaviour of a real material would be expected to fall between these bounds.

A set of values of the physical properties for the highly oriented polymer is required to calculate the compliance coefficients for a unit cell. Since we have not performed definitive experiments ourselves to obtain the full set of properties, we used the published values¹² for ultra-high modulus PE which are listed in *Table 1* (column A).

The modulus predictions from data A are shown in *Figure 6*, where both the compliance and the stiffness calculations are superimposed on the experimental tensile modulus data. In this case much of the experimental data falls outside the bounds imposed by the theoretical curves, and the predicted value for the isotropic polymer ($\lambda = 1$) is between 3 and 20 GPa, compared to an experimental observed value of 1.2 GPa.

A modified set of physical parameters was also used

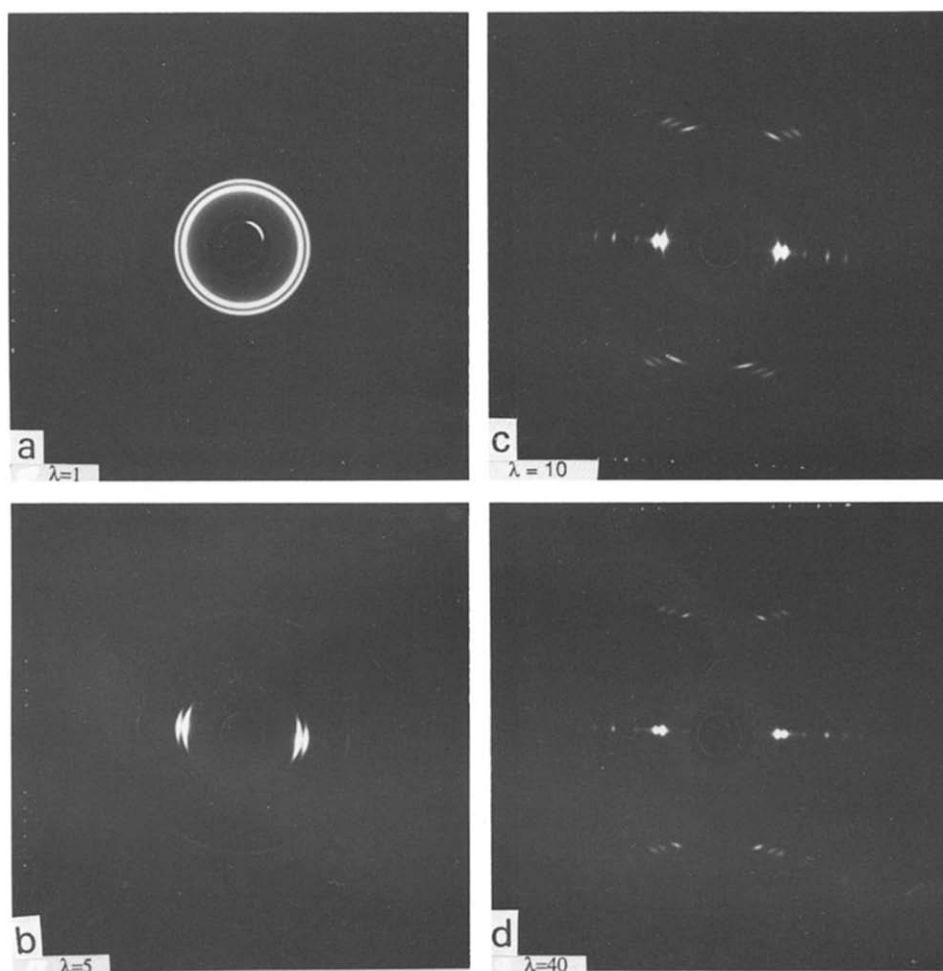


Figure 3 Wide angle X-ray photographs of pre-swollen drawn UHMWPE with draw ratios λ of (a) 1.0, (b) 5.0, (c) 10.0 and (d) 40.0. The drawing direction is vertical

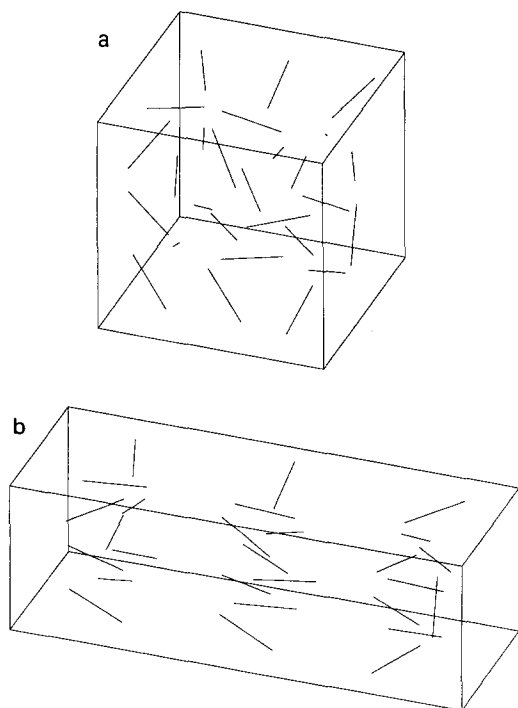


Figure 4 Schematic diagram showing the pseudo-affine deformation applied to the orientations of units in the aggregate: (a) initial stage, with random orientations; (b) after a draw ratio of 2 has been applied

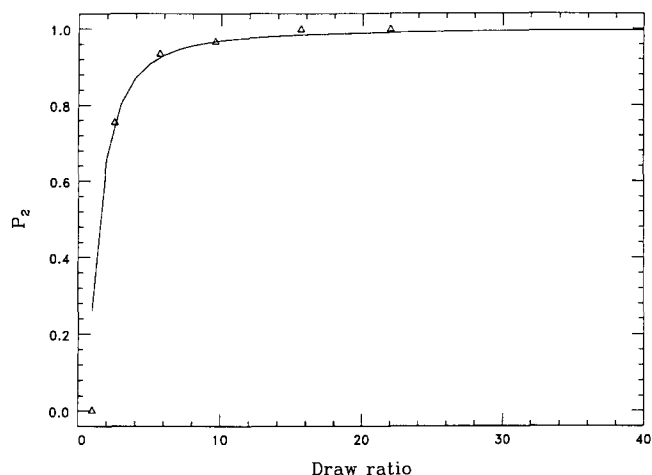
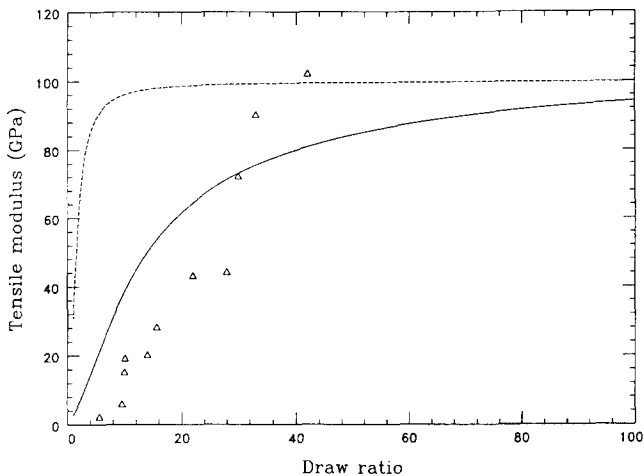
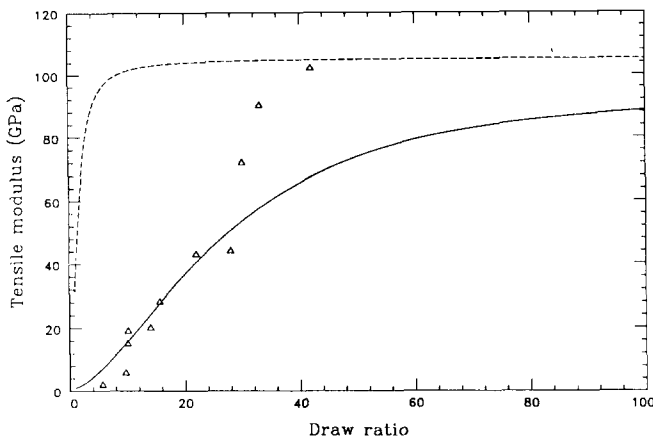
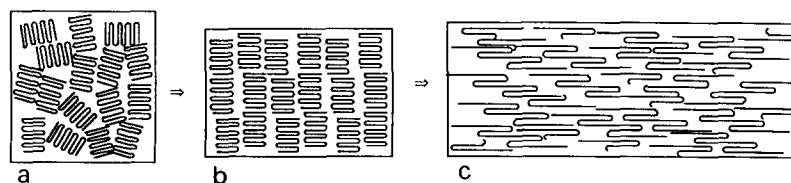


Figure 5 Orientation function as calculated from X-ray diffraction data and calculated using an aggregate model. Δ , Experimental data; —, calculated data

(Table 1, column B). E_{long} was chosen to correspond to the tensile modulus of the highest drawn sample that we generated ($\lambda = 42$). E_{tran} and G were then calculated so that the predicted values of the isotropic moduli, E_{iso} and G_{iso} , obtained using averaging of compliance coefficients were equal to the experimental values measured from undrawn samples ($E_{\text{iso}} = 1.2$ GPa, $G_{\text{iso}} = 0.38$ GPa). It was not possible to obtain realistic values of E_{tran} and G by averaging stiffness coefficients.

Table 1 Values of physical constants used in the simulations shown in Figures 6 and 7^a

			A ^b	B ^c
Tensile modulus perpendicular to symmetry axis (GPa)	E_{tran}	$1/s_{11}$	1.35	2.5
Tensile modulus parallel to symmetry axis (GPa)	E_{long}	$1/s_{33}$	100	105
Shear modulus (GPa)	G	$1/s_{44}$	1.3	0.2
Poisson's ratio	ν_{13}	$-s_{13}/s_{33}$	0.5	0.5
Poisson's ratio	ν_{12}	$-s_{12}/s_{11}$	0.5	0.5

^a Room temperature values quoted, $T = 20^\circ\text{C}$ ^b Values used for Figure 6 obtained from Reference 12^c Values used for Figure 7, adjusted as described in the text**Figure 6** Tensile modulus as experimentally measured (Δ) and as calculated by an aggregate model, using compliance data derived from physical constants given in Reference 12 (Table 1, column A). The two theoretical curves correspond to the averaging of either compliance (—) or stiffness coefficients (---)**Figure 7** Tensile modulus as experimentally measured (Δ) and as calculated by an aggregate model, using compliance data derived from modified physical constants as described in the text (Table 1, column B). The two theoretical curves correspond to the averaging of either compliance (—) or stiffness coefficients (---)**Figure 8** Schematic diagram showing suggested behaviour of swell-drawn polyethylene. (a) Initially the polymer consists of a random arrangement of crystallites. (b) At low draw ratios these crystallites align along the draw direction, leading to an improved orientation function. (c) At higher draw ratios the polymer chains extend along the draw direction, increasing the tensile modulus, but not affecting the orientation function.

Theoretical curves obtained from these modified data are shown in Figure 7, superimposed on the experimental data. It can be seen that the observed mechanical properties follow the lower (compliance average) curve at low draw ratios and then move towards the upper (stiffness average) curve at higher draw ratios. The actual form of the theoretical curves was found to be sensitive to the chosen values of E_{tran} and G but essentially insensitive to varying Poisson ratios.

DISCUSSION

The experimental findings reported in this paper support the results presented in the initial publication on the swelling drawing process¹¹ and show some similarities to results published on gel drawn UHMWPE fibres¹². Molecular orientation measured from X-ray data increases with increasing draw ratio and appears to follow closely that expected from the pseudo-affine deformation of an aggregate of crystals. Most of the orientation is achieved in the early stages of deformation, say up to a draw ratio of order 3–4. Beyond this point $P_2(\theta)$ changes very little. The fact that the simulated value of $P_2(\theta)$ fits the experimental data so well is at first sight a surprising result because it is clear, for example from the SEM observations, that major structural changes are occurring during the deformation process.

The mechanical property data, when compared with simulated values in Figures 6 and 7, suggest that the material properties change from the lower bound behaviour to upper bound behaviour with the imposition of mechanical drawing. The initial lower bound behaviour suggests that the anisotropic units are coupled in a series sense with stress continuity at low deformations and are coupled in a parallel sense with strain continuity at high deformation levels.

The combined orientation and mechanical results suggest to us that at low deformations the dominant effect is crystal orientation, while at high deformations the changing mechanical properties suggest that chain extension rather than orientation is occurring. A schematic interpretation of events that could occur on drawing is shown in Figure 8. Clearly the detailed mechanisms associated with the drawing process are more complicated than drawn in the diagram and the additional aspect that the material becomes highly fibrillar also needs to be taken into account. However, the results do suggest that the enhanced drawability associated with pre-swollen UHMWPE is mainly connected with a chain extension process rather than chain orientation at the later stages of drawing.

The pseudo-affine deformation model appears to be surprisingly successful in describing the drawing behaviour of pre-swollen UHMWPE samples. The fitting

of the aggregate model is sensitive to the values chosen for the elastic constants of the anisotropic units and at present there is some uncertainty on the exact values that should be chosen. When this issue has been resolved a more detailed analysis may be possible. Our scanning electron microscopy results show clearly that a major change in morphology occurs during deformation and the development of fibrillar structure in the draw direction becomes dominant at high draw ratios. This, together with an anticipated increase in crystallinity within the material, can be expected to make accurate molecular modelling of the mechanical drawing process complicated and difficult. It could in principle be possible to introduce some of these factors into the aggregate modelling but at this stage the introduction of further adjustable parameters seems unjustified.

REFERENCES

- 1 Zwijnenburg, A. and Pennings, A. J. *Colloid Polym. Sci.* 1976, **254**, 868
- 2 Smith, P. and Lemstra, P. J. *J. Mater. Sci.* 1980, **19**, 505
- 3 Lemstra, P. J., Van Aerle, N. A. J. M. and Bastiansen, C. W. M. *Polym. J.* 1987, **19**, 85
- 4 Kirschbaum, R., Van Dingenrn, J. L. J. 'Integration of Polymer Sci. and Technology', Proceedings of Rolduc Conference, Elsevier Applied Sciences, London, 1988
- 5 Anton, C., Mackley, M. R. and Solbai, S. B. *Polym. Bull.* 1987, **17**, 175
- 6 Kanamoto, T., Tsurata, A., Tanaka, K., Takeda, M. and Porter, R. *Macromolecules* 1988, **21**, 470
- 7 Kanamoto, T., Ohama, T., Tanaka, K., Takeda, M. and Porter, R. *Polymer* 1987, **28**, 1517
- 8 Ohama, T., Kanamoto, T., Takeda, M. and Porter, R. *Rep. Polym. Phys. Jpn* 1987, 325-328
- 9 Pawlikowski, G. T., Mitchell, D. J. and Porter, R. S. *J. Polym. Sci. Phys.* 1988, **26**, 1865
- 10 Mackley, M. R. and Solbai, S. B. *Polymer* 1987, **28**, 1111
- 11 Mackley, M. R. and Solbai, S. B. *Polymer* 1987, **28**, 1115
- 12 Ward, I. M. *Adv. Polym. Sci.* 1985, **70**, 12
- 13 Peterlin, A. *Colloid Polym. Sci.* 1987, **265**, 357
- 14 Termonia, Y. and Smith, P. *Macromolecules* 1988, **21**, 2184
- 15 Stein, R. S. *J. Polym. Sci.* 1958, **21**, 327
- 16 Ward, I. M. 'Mechanical Properties of Solid Polymers', Wiley, 1971, Ch. 10
- 17 Raumann, G. and Saunders, D. W. *Proc. Phys. Soc.* 1961, **77**, 1028
- 18 Bishop, J. and Hill, R. *Phil. Mag.* 1951, **42**, 414, 1248

APPENDIX

The crystal orientation functions are defined as:

$$f_{\alpha} = \frac{1}{2} \langle 3 \cos^2 \alpha - 1 \rangle \quad (\text{A1})$$

$$f_{\beta} = \frac{1}{2} \langle 3 \cos^2 \beta - 1 \rangle \quad (\text{A2})$$

$$f_{\varepsilon} = \frac{1}{2} \langle 3 \cos^2 \varepsilon - 1 \rangle \quad (\text{A3})$$

where α , β , and ε are the angles measured between the z axis (the stretching direction) and the a , b and c crystallographic axes, respectively. f_{ε} is normally used for describing crystal orientation function, i.e. $P_2(\theta)$.

To determine the f s from the X-ray pattern, it is most convenient to work with the 200 and 020 reflections. The orientations of the crystals giving rise to the diffraction at these points are given by equations

$$\cos \alpha = \cos \theta_{200} \sin \phi_{200} \quad (\text{A4})$$

and

$$\cos \beta = \cos \theta_{020} \sin \phi_{020} \quad (\text{A5})$$

where θ_{200} and θ_{020} are the Bragg angles for the 200 and 020 reflections. The angles ϕ_{200} and ϕ_{020} are measured from the equator to a point on the two arcs.

Substituting equations (A4) and (A5) into equations (A1) and (A2), one obtains:

$$f_{\alpha} = \frac{1}{2} \langle 3 \cos^2 \theta_{200} \overline{\sin^2 \phi_{200}} - 1 \rangle \quad (\text{A6})$$

$$f_{\beta} = \frac{1}{2} \langle 3 \cos^2 \theta_{020} \overline{\sin^2 \phi_{020}} - 1 \rangle \quad (\text{A7})$$

The values of $\overline{\sin^2 \phi}$ may be computed from the following equation:

$$\overline{\sin^2 \phi_{200}} = \frac{\int_0^{\pi/2} I(\phi_{200}) \sin^2 \phi_{200} \cos \phi_{200} d\phi_{200}}{\int_0^{\pi/2} I(\phi_{200}) \cos \phi_{200} d\phi_{200}} \quad (\text{A8})$$

where $I(\phi_{200})$ is the relative intensity around arc (200) and was experimentally determined as described in this paper. The c axis orientational function is given by

$$P_2(\theta) = f_{\varepsilon} = 1 - f_{\alpha} - f_{\beta} \quad (\text{A9})$$